PAN
ARCHIVES OF ACOUSTICS
Vol. **46**, No. 1, pp. 31–40 (2021)
DOI: 10.24425/aoa.2021.136558

Research Paper

The Effect of Sonication Parameters on the Thickness of the Produced MoS_2 Nano-Flakes

Najme Sadat TAGHAVI, Reza AFZALZADEH*

Faculty of Physics
K. N. Toosi University of Technology
Tehran 15418-49611, Iran
*Corresponding Author e-mail: afzalzadeh@kntu.ac.ir

(*received March 20, 2020; accepted October 31, 2020*)

Liquid Phase Exfoliation (LPE) is a common route to produce two-dimensional MoS_2 nanosheets. In this research, MoS_2 powder is exfoliated by an ultrasonic probe (sonicator) in a water-ethanol solution. It is reported that MoS_2 as a prototype 2D Transition Metal Dichalcogenide, has a band gap that increases with a decreasing number of layers. There are some factors that affect the average band gap energy value and the thickness of the exfoliated flakes. We varied different parameters of the ultrasonic probe like power, pulse percentage and time duration of sonication to investigate the effects on the number of MoS_2 layers. Our findings from the UV-Visible spectra, SEM, FESEM and TEM images indicate that the minimum thickness for these samples was acquired at 50% of the input power of the sonicator we used (~65 W) and the optimum pulse percentage is 50%. The current study also found that the average amount of band gap increased with an increase in sonication time, and then remained unchanged after 60 minutes.

Keywords: ultrasonic probe; 2D MoS_2 band gap; power output; pulse percentage, sonication time.

1. Introduction

Molybdenum Disulfide (MoS_2) is a Transition Metal Dichalcogenide (TMD). TMDs are one of the most studied classes of layered materials (Mas-Ballesté *et al.*, 2011; Butler *et al.*, 2013; Miró *et al.*, 2014). TMDs have received indicative interest because they show unique mechanical, electrical, and optical properties (Wang *et al.*, 2014; Zhang *et al.*, 2016; Wang *et al.*, 2015). MoS_2 nanosheets have been widely studied for a broad range of applications in electronics, optoelectronics, sensors, catalysis, and energy storage (Han *et al.*, 2015; Wang *et al.*, 2012). MoS_2, like graphene, is a two-dimensional (2D) layered material, with a covalently bonded hexagonal lattice in layers stacked by weak van der Waals interactions between sheets (Butler *et al.*, 2013; Wang *et al.*, 2015; Han *et al.*, 2015). But unlike graphene, the monolayer of MoS_2 as a semiconductor shows a transition from the bulk indirect band gap of ~1.2–1.3 eV, to a direct band gap of ~1.8–1.9 eV (Wang *et al.*, 2012; Samadi *et al.*, 2018; Mak *et al.*, 2010). One of the most intriguing features of MoS_2, as a 2D crystal, is that its band gap depends on the number of layers (Samadi *et al.*, 2018; Mak *et al.*, 2010; Niu *et al.*, 2018).

Having strong in-plane bonds and weak out-of-plane interactions, enables this class of layered materials to be exfoliated into 2D sheets (Mas-Ballesté *et al.*, 2011; Wang *et al.*, 2012). There are several various routes for exfoliation of TMDs (Choi *et al.*, 2017; Yang *et al.*, 2018; Brent *et al.*, 2017). These approaches can be divided into two classes:

1) the methods that result in high quality and large area sheets on substrates, such as Chemical Vapor Deposition (CVD) method (Zhang *et al.*, 2016; Wang *et al.*, 2015; Choi *et al.*, 2017);
2) the methods which produce a large number of small nanoflakes, such as Liquid Phase Exfoliation (LPE) technique (Yang *et al.*, 2018; Brent *et al.*, 2017; Babu Arumugam *et al.*, 2019; Song *et al.*, 2013). LPE, like other solution-based methods, is an easy to implement, versatile and simple yet powerful method (Zhang *et al.*, 2016; Backes *et al.*, 2017; Huo *et al.*, 2015; Coleman *et al.*, 2011; Nicolosi *et al.*, 2013).

The irradiation of a liquid medium with the ultrasound of sufficient pressure causes the formation, growth, oscillation and implosive collapse of bubbles. This high energetic transient process and its physical effects (like shock waves), known as acoustic cavitation, is the root cause of sonochemical experiments such as ultrasound-assisted exfoliation (Pokhrel *et al.*, 2016; Bang *et al.*, 2010; Xu *et al.*, 2013). MoS_2 can be delaminated in liquid phase utilizing ultrasonic probe to extract individual layers (Backes *et al.*, 2017; 2020; Jawaid *et al.*, 2016). The LPE process, which is a top-down approach, generally consists of 3 main steps: I) dispersion of precursors in a proper solvent, II) exfoliation in solution by a sonicator (for brevity called "sonoexfoliation"), and III) purification or separation of exfoliated from non-exfoliated flakes through centrifugation (Song *et al.*, 2013; Backes *et al.*, 2017).

Several research groups have studied the role of effective parameters on LPE procedure results. Coleman group investigated the different conditions for sonoexfoliation of graphene and TMD nanosheets (Coleman *et al.*, 2011). They also presented a novel centrifugation process for separating the 2D flakes depend on differences in the size and the thickness of them (Brent *et al.*, 2017). Qiao *et al.* (2014) examined the influence of ultrasonic cavitation intensity on the concentration and morphology of MoS_2 nanoflakes in N-methyl-2-pyrrolidone (NMP) solvent. The effect of applied acoustic power and the ultrasound frequency on the mean bubble size in water were studied by Brotchie *et al.* (2009). Merouani and colleagues performed a theoretical study on the influence of ultrasound frequency and acoustic amplitude on the ambient bubble radius in sonochemical reactions (Merouani *et al.*, 2013). Han *et al.* (2015) examined the effect of some ultrasound parameters such as amplitude and probe immersion depth on the power and the acoustic flow rate in the sonication treatment. Shen *et al.* (2015) obtained the accurate surface tension components of about 40 solvents and their compounds. Also, they studied the matching of surface tension components between solvents and the precursors. Peng *et al.* (2015) examined the impact of pH value on sonoexfoliation of MoS_2 in Graphene oxide (GO) suspension. GO plays the role of surfactant in their approach. Using a cascaded centrifugation procedure, Kajbafvala *et al.* (2018) presented a new technique for selecting the MoS_2 flakes with different lateral sizes and thicknesses. The effect of concentration of the starting material on the final concentration of dispersions was investigated by Green group. Their study indicates that spray drying can lead to crumpled morphology for boron nitride, MoS_2, and WS_2 nanoflakes (Bari *et al.*, 2015). A number of researchers explored the impact of selected solvents (with or without additives) on the achievement in the exfoliation process as well (Babu Arumugam *et al.*, 2019; Jawaid *et al.*, 2016; Nguyen *et al.*, 2015; Kiełczyński *et al.*, 2019).

The obtained flakes can be readily separated and scalable. An essential step during the fabrication procedure and before using the generated nanoflakes in any application is the characterization. Many various characterization methods (like UV-Visible, photoluminescence, and Raman spectroscopy, X-Ray diffractometry, Field Emission Scanning Electron Microscopy (FESEM), and Transmission Electron Microscopy (TEM)) can be used in order to study the properties of products (Wang *et al.*, 2012; Backes *et al.*, 2017).

In this research study, MoS_2 flakes are prepared via LPE method utilizing an ultrasonic probe. We investigated the variation effects of the power, the pulse duration and the time duration of the sonicating process.

2. Experimental

2.1. Materials and methods

All the chemicals used in this study were research grade and deionized water was used throughout the experiments. The sonication was carried out using ultrasonic processor with titanium probe of 14 mm in diameter (FAPAN-400R model made in Iran by FAPAN Co. Ltd.) with operation frequency of about 24 kHz, and nominal power of 400 W. The ultrasound processor is capable of variation in power in 10 equal steps, also pulse duration in 10 steps to choose irradiation on-off in percentage.

2.2. Sample preparation

All samples were prepared via immersing 100 mg MoS_2 bulk powder in ~60 ml of water-ethanol solutions (a mixture of 77% DI water and 23% ethanol by volume) in a 100 ml glass beaker. We aim to utilize a "green solvent" in order to minimize the environmental impacts. As expected, water is the greenest solvent (Marcus, 2018). But, water has surface tension of about 72 mN/m at 25°C, while it is frequently reported that the proper value of surface tension for sonication treatment of MoS_2 in liquid phase is about 40 mN/m (Coleman *et al.*, 2011; Nguyen *et al.*, 2015; Ghasemi *et al.*, 2016). So, it was necessary to add another green solvent to water to reduce surface tension. We choose ethanol because it is proved that ethanol, as simple alcohol, is also an environmentally preferable solvent (Capello *et al.*, 2007). The (77/23) volume ratio for (DI water/ ethanol) was calculated using the Connors-Wright equation for making binary aqueous-organic solutions (Connors *et al.*, 1989).

The mixture was sonicated applying a 14 mm diameter ultrasonic probe (FAPAN-400R). The beaker was put in an ice-water bath to avoid evaporation of

ethanol due to increasing the temperature of the solution during the sonoexfoliation process. Furthermore, the sonicator was adjusted to pulse mode for X fraction of a second "on" and (1-X) fraction of second "off" to prevent overheating the solution and impairing the sonicator processor. So, the total sonication time for preparing the samples is: (60/X) minutes in "on" state.

The last step which is necessary to separate exfoliated from un-exfoliated flakes is centrifugation. We eliminated thick flakes by 2 steps centrifugation using a benchtop centrifuge: the first step was done for 45 minutes at 3000 rpm (rotations/minute) and then the top 2/3 (th) of the dispersion was retained for the next step and the rest of the liquid was discarded. Afterwards, the second step was carried out again for 30 minutes at 3600 rpm, and finally, the top 75% of the supernatant was collected for the following analyses (Qiao *et al.*, 2014).

3. Results and discussion

In this section, the effects of different varied parameters like power, pulse duration and the total sonication time on the exfoliation process of MoS_2 is presented and discussed.

3.1. Effect of sonicator power on the exfoliation

The MoS_2 dispersions were prepared by utilizing an ultrasonic probe in water-ethanol solution at various power percentage of the sonicator in 20%, 40%, 50%, 70%, and 90% equivalent to 38.5, 47, 65.5, 84, and 96.8 watts in one-hour duration (see the Supplementary Information). The probe was pulsed for half a second "on" and half a second "off" to avoid excessive heating. We studied the effect of changing the power of sonicator in detail by measuring their UV-Vis. absorption spectra and Scanning Electron Microscopy.

The optical characterization of the MoS_2 sheets was performed with a Perkin-Elmer Lambda 25 spectrometer. Using the absorption spectrum (precisely the position of peak A) obtained from UV-Vis spectrometer one can calculate the band gap energy of 2D materials and estimate the approximate thickness of the layers, or equally the approximate number of layers. The UV-Vis. absorption spectra of MoS_2 samples for 20%, 40%, 50%, 70%, and 90% of the maximum power of the sonicator are shown in Fig. 1. In each spectrum, as a characteristic spectrum for MoS_2, the excitonic peaks around 669 nm (ascribed to A peak) and ~609 nm (ascribed to B peak) are emerging due to a direct gap transition at the K-point of the Brillouin zone in 2D MoS_2. The A-B splitting arises from the combined effect of interlayer coupling and the splitting of the valence band due to spin–orbit coupling (Vella *et al.*, 2016; Frisenda *et al.*, 2016; Song *et al.*, 2013). The other peaks, i.e. C and D, could be attributed to

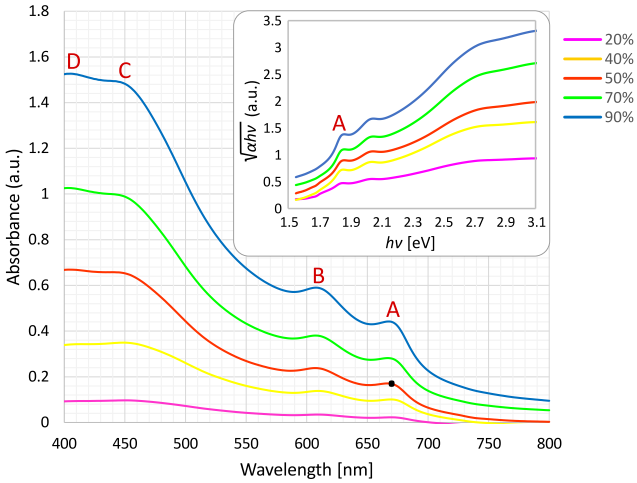

Fig. 1. The UV-Visible absorption spectrum for MoS_2 flakes prepared with different sonicator powers. The inset shows the Tauc plots for the different powers which were utilized to calculate the band gap energy of each dispersion.

the direct transition from the deep valence band to the conduction band (Vella *et al.*, 2016).

Tauc plot was utilized to determine the optical band gap of MoS_2 flakes. A Tauc plot essentially shows the amount of $(\alpha h\nu)^{1/r}$ versus the energy of the light ($h\nu$) in eV, where α is the absorption coefficient of the material and $r = 2$ for our MoS_2 samples, because of indirect allowed transitions (Voshell *et al.*, 2018; Zhu *et al.*, 2016).

As can be seen in Fig. 2, the graph shows that there is an almost sharp increase in the average band gap energy of dispersions in the first half of the graph, and a gentle decrease in the second half. So, the best result is referred to the power output of 65.5 W (50% of the maximum power) in the middle of the graph. The observed increase in the first half of the graph could be attributed to the fact that the required energy for overcoming the van der Waals forces between layers is provided easier by raising the power and hence the quantity of monolayers grows. And in the second half of the graph (or right-hand side of the graph), it seems that this decrease is due to the agglomeration of nanosheets.

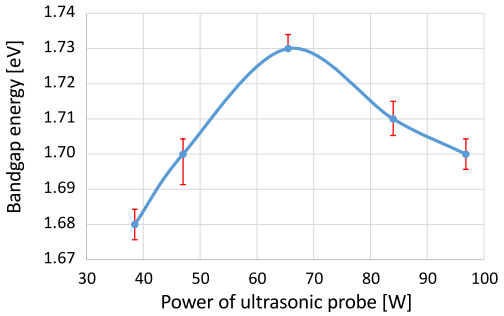

Fig. 2. Variation of the band gap energy of MoS_2 samples as a function of power of the sonicator.

This result were also confirmed by SEM images as shown in Fig. 3.

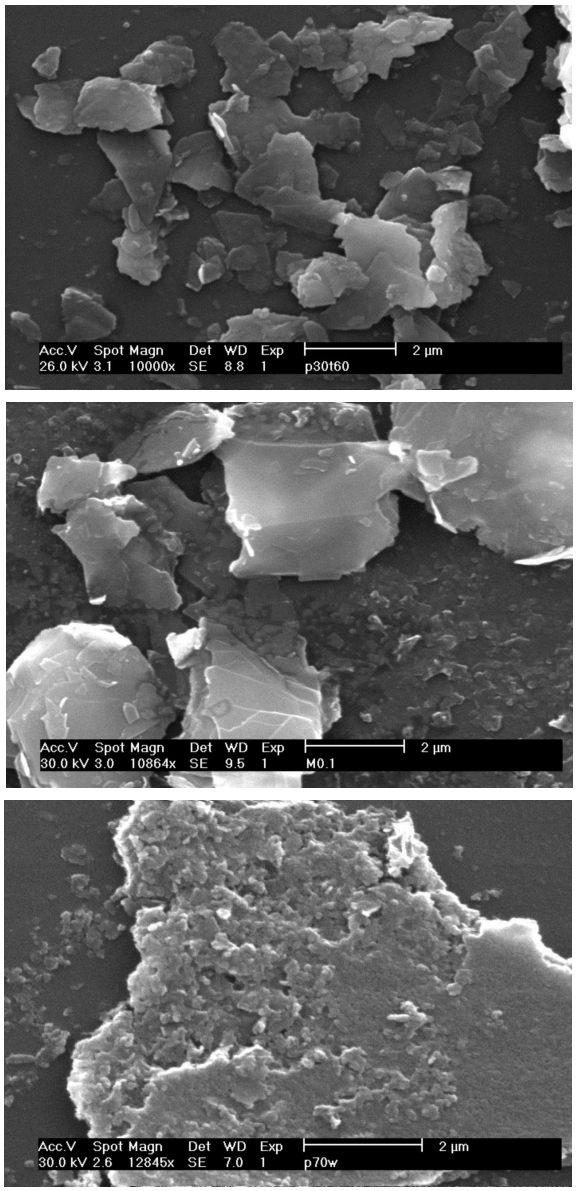

Fig. 3. SEM micrographs of MoS_2 flakes produced at: a) 47 W, b) 65.5 W, and c) 84 W (scale bars: 2 µm).

Additionally, it can be seen from Fig. 3 that at the power of 65.5 W, the lateral sizes (or the area) of flakes and the quality of them increased compared to the previous and the next samples. At 47 W, the flakes are smaller and relatively thicker. At 65.5 W, the dimensions of flakes are about twice the size of samples exfoliated at 47 W. But at 84 W, it seems that the flakes completely lost their quality because of the agglomeration phenomenon. This agglomeration at higher power is due to the high energetic bubble collapse (Kudryashova *et al.*, 2019). Exfoliated sheets surrounding a high energetic bubble, after the collapse of the bubbles, collide with each other and reverse-exfoliation (agglomeration) occurs (Fig. 4).

Another important point is the ultrasonic power applied for exfoliation. Higher power will cause an increase in the size and number of bubbles. Larger bubbles consist of more air and/or gases. So, the medium, in which the ultrasonic probe operates, changes from liquid to gaseous phase in some zones. Therefore, ultrasound travels (about 4.5 times) slower in these zones than in the liquid. In such a situation, the effects of shock waves, which are the most important physical effects of sonication, are reduced while the force of bubble implosion increases. These implosive collapses will damage the nanosheets and reduce the size of the flakes. This leads to the lower efficiency for sonication power more than 65.5 W in the present research set up.

3.2. Effect of sonicator pulse duration on the exfoliation

In order to investigate the effects of pulse percentage, the MoS_2 dispersions were produced in water-ethanol mixtures at the power of 65.5 W for one hour in "on" state (60 min is the effective time and the total sonication times are shown in Table 1). It is because the total sonication time multiplied by pulse percentage presents an effective time. The effect of changing the pulse duration, i.e. on/off ratio of the ultrasonic

Table 1. The total applied sonication time and the band gap energy of MoS_2 samples obtained as a function of the probe pulse duration. Effective time is 60 min for all cases.

Pulse percentage of probe [%]	30	50	60	70	90
Total sonication time [min]	200	120	100	86	67
Band gap energy [eV]	1.72	1.73	1.72	1.71	1.71

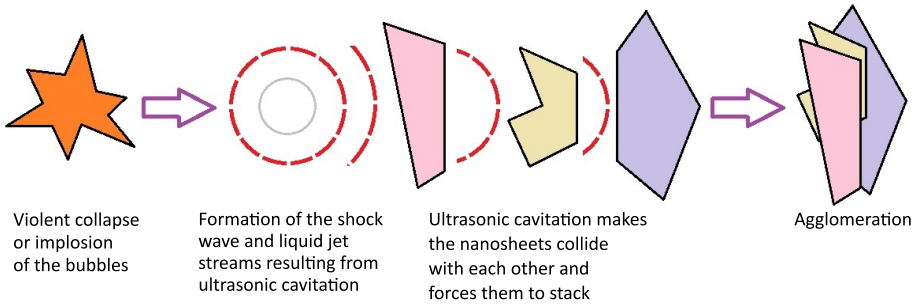

Fig. 4. A schematic representation of the effect of ultrasonic cavitation on the dispersed nanosheets in the liquid phase.

probe for 30%, 50%, 60%, 70%, and 90%, was studied in detail by measuring the UV-Vis absorption spectra of the solutions (Fig. 5). The applied percentages of "on" state of the probe and their measured band gap energy amounts are shown in Table 1. As can be seen, the band gap energy and thus the probability of making monolayer increase as the pulse percentage increases up to 50% due to increasing the opportunity to delaminate MoS_2 flakes. Above 50% of the observed results show a decrease in band gap energy. It could be attributed to more turbulent and quick flows which provide more contacts between MoS_2 sheets. These encounters enhance the possibility of agglomeration. After decreasing the band gap energy, the foregoing effective factors balance each other out, therefore the average amount of band gap energy remains relatively constant. Tauc plots for the different pulse percentage (shown in the inset of Fig. 5) are traced for calculation of band gap energy of each dispersion.

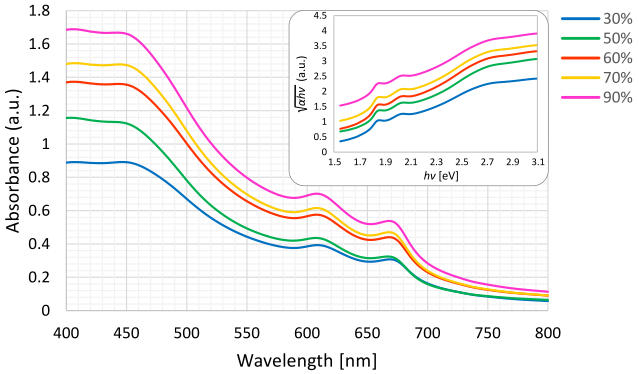

Fig. 5. The UV-Visible absorption spectrum for MoS_2 flakes prepared at power of 65.5 W for different pulse percentage. The inset shows the Tauc plots for the different pulse percentage which are utilized to calculate band gap energy of each dispersion.

3.3. Effect of sonication time on the exfoliation

To study the influence of the effective time of sonication, the dispersions were prepared in water-ethanol solutions at 65.5 W in different sonication time durations of 15, 30, 60, 120, and 180 min (Fig. 6). The probe was pulsed for half a second "on" and half a second "off". From Fig. 7, we can see that the average amount of band gap energy increases gradually with an increase in effective sonication durations up to 60 min and then remains constant. An explanation for the observed raising might be that long exposure time provides more occasions for delamination of more flakes. Above 60 minutes there would again be a competition between increasing factors and the tendency for nanosheets to aggregation with each other. Therefore, one could see that after 1 h, the average amount of band gap energy finally stops increasing.

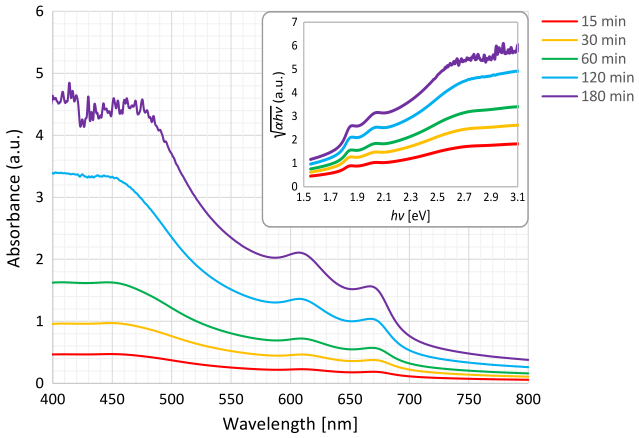

Fig. 6. The UV-Visible absorption spectrum for MoS_2 flakes prepared at the power of 65.5 W for different sonication time durations. The inset shows the Tauc plots for the different sonication durations which are utilized to calculate the band gap energy of each dispersion.

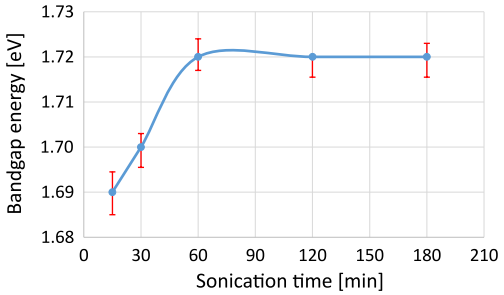

Fig. 7. The measured energy band gap of the MoS_2 samples as a function of effective sonication time.

The SEM micrographs shown in Fig. 8, confirm the results mentioned above. As can be seen, the flakes in Fig. 8b are larger and thinner than the flakes in Fig. 8a. It seems that by increasing the effective sonication time from 15 to 60 min, the exfoliation occurred better. But, above 60 min, the quality of flakes decreases because of the agglomeration process. Figure 8c shows agglomeration and crushing the flakes simultaneously.

All findings in this research result in the fact that our finest MoS_2 samples were acquired at 65.5 W, the pulse of 50% "on", and 60 min irradiation duration. So, we call this situation "the optimum situation" and the fabricated samples in such a situation (power, pulse, and duration) are called "the optimum samples" henceforward.

As a quantitative assessment, we can use the following beneficial semi-empirical equation:

$$N = 2.3 \times 10^{36} e^{-54888/\lambda_A}, \tag{1}$$

where N is the mean number of monolayers per nanosheet and λ_A (in nanometer) is the measured A-exciton wavelength (Kajbafvala *et al.*, 2018; Backes *et al.*, 2014).

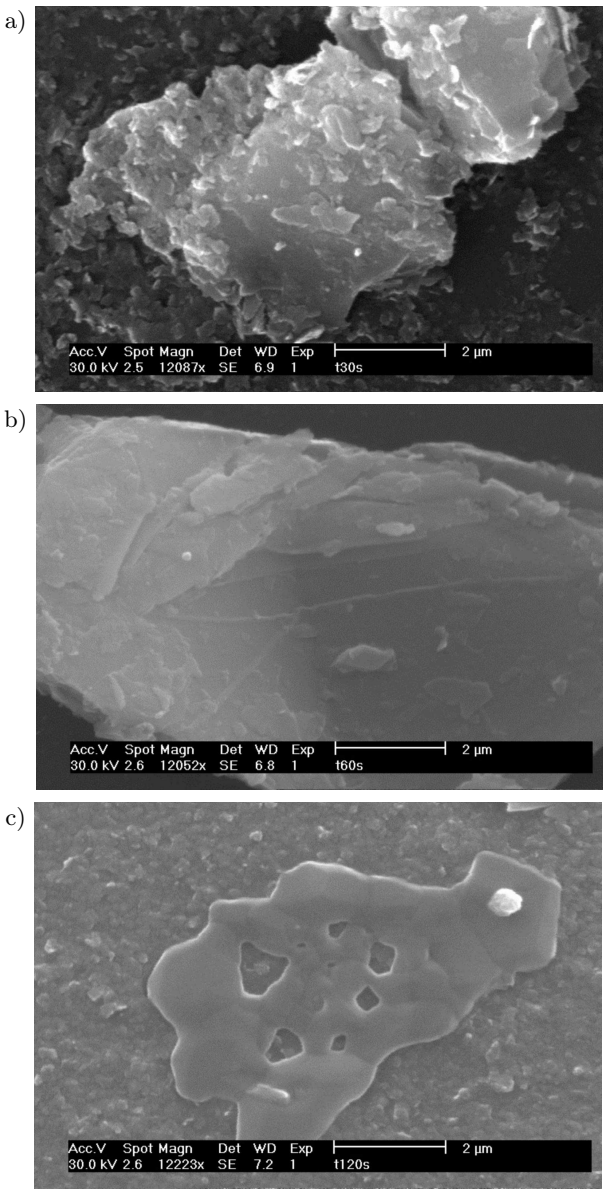

Fig. 8. SEM micrographs of MoS_2 flakes refer to: a) 30 min, b) 60 min, and c) 120 min sonication time (scale bars: 2 µm).

For our optimum sample, with $\lambda_A = 666.5$ nm (see the black point in Fig. 1), the average number of layers will be $N \sim 4$ layers. So, it seems that it is a fairly acceptable result with a green, non-expensive and additive-free solution.

To further characterize the microstructure of MoS_2, the crystallographic pattern of the standard sample was achieved using XRD method, as shown in Fig. 9. The phase of MoS_2 nanosheets is confirmed to be a hexagonal structure belonging to the space group P63/mmc (point group D_{6h}) with 2 MoS_2 molecules inside the unit cell as indexed by standard card number 01-087-2416. The XRD analyses were performed utilizing an X'Pert PRO MPD PANalytical Company diffractometer.

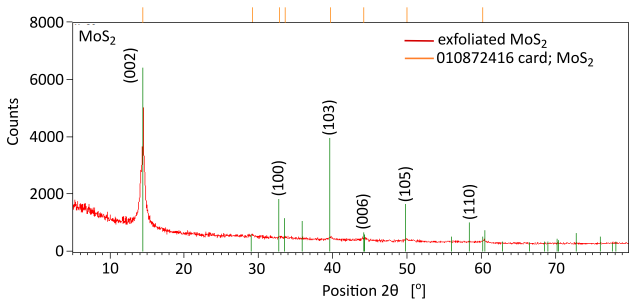

Fig. 9. XRD pattern of the optimum sample of the MoS_2 exfoliated.

As can be seen from Fig. 9, the strongest peak is the peak of (002) plane at $2\theta = 14.436°$. This peak is evidence for the existence of the superlattice. Comparing the exfoliated with the unexfoliated MoS_2 XRD data showed that the sharpness, strength, and height of this peak had been reduced due to exfoliation process because of decreasing the size of flakes (Liu *et al.*, 2013; Tonndorf *et al.*, 2013; Nguyen *et al.*, 2016).

The morphology of MoS_2 nanosheets was studied by a Field Emission Scanning Electron Microscopy (FESEM, TESCAN mira3 (15 Kv)). Figure 10 shows

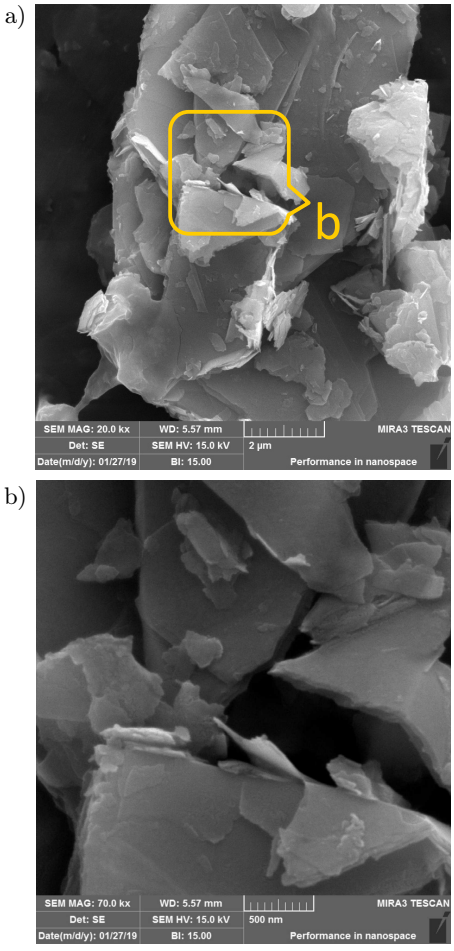

Fig. 10. FESEM micrographs of MoS_2 nanoflakes; scale bar: a) 2 µm, b) 500 nm.

the FESEM images of MoS_2 flakes, which exhibit the typical lamellar structure of our standard sample.

The structural characterization of the MoS_2 nanosheets was further examined by Transmission Electron Microscopy (TEM, Zeiss EM900 (80 Kv)). Figure 11 shows the TEM images of our optimum sample prepared by the LPE method. The TEM analysis results confirmed the layered structure of the MoS_2 nanosheets. In Fig. 11a, a rectangular nanoflake with approximate dimension of 800×500 nm is observed with very high transparency.

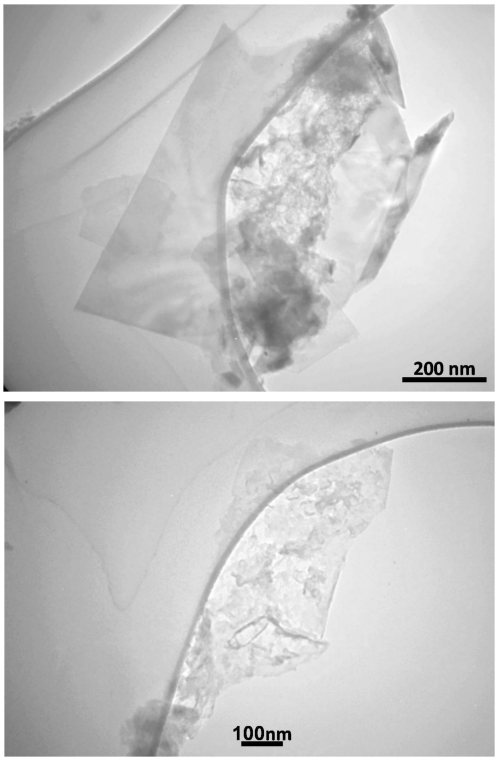

Fig. 11. TEM micrographs of MoS_2 flakes, scale bar: a) 200 nm, b) 100 nm.

4. Conclusion

In this research work, we successfully prepared MoS_2 few-layers via LPE method by means of an ultrasonic probe in different conditions. The dispersions were produced through immersing bulk molybdenum disulfide (MoS_2) powder to water-ethanol solvent as a green, low-cost, available and non-toxic solution. In this research, some effective parameters, including sonicator's power, pulse percentage, and sonication time, on the average band gap energy of the obtained MoS_2 ultra-thin flakes were studied. Based on our findings from UV-Vis. Spectroscopy and SEM micrographs, the optimum operating parameters of our ultrasonic transducer to achieve ultra-thin flakes were obtained at 65.5 W of power output, 50% of pulse percentage (for "on" states), and 60 min of sonication time (for probe 14 mm in diameter). Lastly, the structure, morphology, and the average thickness of the optimal sample were probed by XRD, FESEM, and TEM imaging. For our optimum sample, the average number of layers per flake is expected to be 4.

Appendix. Supporting information

Measuring the power of ultrasonic system

There are several physical or chemical methods to determine ultrasonic power. Some widely used approaches are calorimetry (physical methods) and KI dosimetry (chemical method). We used these 2 methods to evaluate the power of our sonotrode.

The physical approach: Calorimetry

Calorimetry is the method of measuring the amount of thermal energy exchanged during a physical procedure or chemical reaction. This is the process of calculation of the temperature conversion that happens during the operation and the masses of the system and surroundings. Subsequently, one can use these results as inputs of an equation for computing the amount of heat released or absorbed in the process.

The chemical approach: KI dosimetry

Iodide dosimetry is also a proposed method of calibration of ultrasonicpower, which generate reliable and reproducible results. Assessment of cavitation efficiency through the Potassium iodide (KI) dosimetry method, is based on the fact that KI dissociated to K^+ and I^- ions, and during ultrasonication, oxidation occurs and iodide (I^-) ions can be transformed into diatomic iodine molecule (I_2). The additional I^- ions existing in solution react with I_2 and form I_3^- ions. By measuring the absorbance of I_3^- ions via UV-Vis. Spectrometer at 350 nm, it is possible to estimate the concentration of I_3^- ions liberated after a sufficient sonication time. The obtained result is a reliable measure of ultrasonic power (Tamura, Miyata, 2015; Ebrahiminia *et al.*, 2013).

Determining the thermal power of system (Calorimetry)

Thermal power consumption of our 14 mm diameter ultrasonic probe (FAPAN 400R, 400 W, 24 kHz) was measured via calorimetry method. For the experiment, 30 cc of deionized water was poured in a 100 ml beaker. The ultrasonic probe immersion depth was 5 mm.

The applied percentage of maximum power (PMP), percentage of pulse ("on" state of the probe), and the sonication durations are shown in Table 2.

The thermometry process was carried out every 15 minutes after irradiation using a temperature controller (Autonics-TZ4ST) and a temperature sensor (PT100). Afterwards, the time-temperature graphs were plotted. Utilizing these graphs, the amount of increased and dissipated power was recorded for 12 time

Table 2. The condition of the calorimetry experiments.

Percentage of maximum power [%]	20, 50, 100
Percentage of pulse [%]	30, 40, 50, 60, 80 100
Sonication time [s]	30, 60, 90, 120, 150, 180, 210, 240, 270, 300, 330, 360

intervals. Averaging those 12 results, we obtained the rate of increase in temperature $(\Delta\theta/\Delta t)$. In order to increase the accuracy, we added $(\Delta\theta/t)_s$ to the previous term, which is the rate of temperature lost due to heat exchanged with the environment (surroundings). So, the amount of thermal power can be calculated using the equation:

$$P_{\text{calorimetry}} = (mc + C')\left(\left(\frac{\Delta\theta}{\Delta t}\right) + \left(\frac{\Delta\theta}{\Delta t}\right)_s\right), \qquad (2)$$

where m is the mass of deionized water; c is the heat capacity of water; and C' is a constant depending on the mass and the type of the beaker and thermometer, which contributed to heat exchange. The subscript s refers to surroundings.

Knowing m and c, and determining the changes in the recorded temperature amounts, the constant C' can be calculated using Eq. (2). These values lead to $C' = 33.53$ J/K.

It is noticeable that the thermometer should not be in the solution during sonication treatment. The first reason is the influence of thermometer on changing the radiation modes in the beaker, and the second one is the possibility of damage to the sensor of thermometer during irradiation (Hajnorouzi *et al.*, 2014).

Calculating the electrical power consumption

The electrical power of ultrasonic probe was measured with a multimeter (Victor 88C). The probe was dipped ~1 cm into the solution and different PMPs were applied. The multimeters were connected in series, and the electrical current consumption was measured. Applying voltage of 220 V, the average power (RMS) was attained. The amount of power of sonotrode *vs* PMP is shown in Fig. 12.

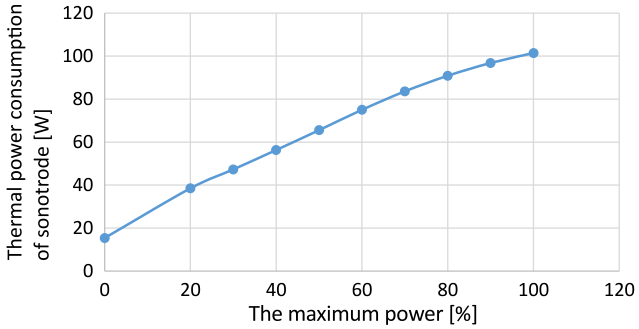

Fig. 12. Thermal power consumption of ultrasonic probe *vs* maximum power.

Table 3. The amount of thermal power consumption of ultrasonic probe and the electric current *vs* maximum power.

The maximum power [%]	The thermal power consumption [W]	The electric current [A]
0	15.40	0.070
20	38.50	0.175
30	47.30	0.215
40	56.32	0.256
50	65.56	0.298
60	75.02	0.341
70	84.04	0.382
80	90.42	0.411
90	96.58	0.439
100	101.20	0.460

KI dosimetry

The most important consequent of ultrasonic irradiation in solution is the collapse of bubbles formed via cavitation. This phenomenon is effectively the cause of generating OH^- free radicals that play a key role in oxidation of I^- ions and formation of I_3^- ions.

50 cc of potassium iodide 0.1 mol was poured in a 100 ml beaker. The probe of the probe was placed 1 cm into the KI solution. The exposure duration was 10 minutes (ten 1-minute intervals). The applied percentage of maximum power was 20, 40, 60, 80, and 100%. For each PMP, a fresh solution was prepared and then exposed under the probe irradiation. Finally, the absorbance of KI solution (equally the concentration of I_3^- ions) measured by a UV-Vis. spectrometer (Perkin-Elmer Lambda 25) at 350 nm, during each time interval. Then, the concentration-time graph was plotted and its slope was calculated. The amount of this slope indicates the concentration of I_3^- ions per minute. The slope of graph *versus* PMPs is shown in Fig. 13. It is

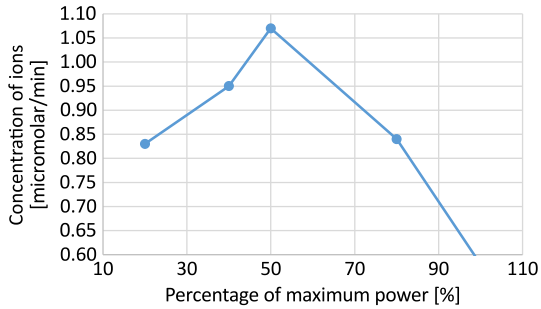

Fig. 13. The concentration of I_3^- ions in solution *vs* the percentage of maximum power of ultrasonic probe.

worth mentioning that during all experiments, to avoid temperature fluctuations, we used a water-bath.

Conflicts of Interest

The authors declare that they have no conflict of interest.

References

1. Babu Arumugam A., Rajamohan V., Bandaru N., Sudhagar P.E., Kumbhar S.G. (2019), Vibration analysis of a carbon nanotube reinforced uniform and tapered composite beams, *Archives of Acoustics*, **44**(2): 309–320, doi: 10.24425/aoa.2019.128494.
2. Backes C. *et al.* (2014), Edge and confinement effects allow in situ measurement of size and thickness of liquid-exfoliated nanosheets, *Nature Communications*, **5**: 4576, doi: 10.1038/ncomms5576.
3. Backes C. *et al.* (2017), Guidelines for exfoliation, characterization and processing of layered materials produced by liquid exfoliation, *Chemistry of Materials*, **29**(1): 243–255, doi: 10.1021/acs.chemmater.6b03335.
4. Backes C. *et al.* (2020), Production and processing of graphene and related materials, *2D Materials*, **7**(2): 022001, doi: 10.1088/2053-1583/ab1e0a.
5. Bang J.H., Suslick K.S. (2010), Applications of ultrasound to the synthesis of nanostructured materials, *Advanced Materials*, **22**(10): 1039–1059. doi: 10.1002/adma.200904093
6. Bari R. *et al.* (2015), Liquid phase exfoliation and crumpling of inorganic nanosheets, *Physical Chemistry Chemical Physics*, **17**(14): 9383–9393, doi: 10.1039/C5CP00294J.
7. Brent J.R., Savjani N., O'Brien P. (2017), Synthetic approaches to two-dimensional transition metal dichalcogenide nanosheets, *Progress in Materials Science*, **89**: 411–478, doi: 10.1016/j.pmatsci.2017.06.002.
8. Brotchie A., Grieser F., Ashokkumar M. (2009), Effect of power and frequency on bubble-size distributions in acoustic cavitation, *Physical Review Letters*, **102**(8): 084302, doi: 10.1103/physrevlett.102.084302.
9. Butler S.Z. *et al.* (2013), Progress, challenges, and opportunities in two-dimensional materials beyond graphene, *ACS Nano*, **7**(4): 2898–2926, doi: 10.1021/nn400280c.
10. Capello C., Fischer U., Hungerbühler K. (2007), What is a green solvent? A comprehensive framework for the environmental assessment of solvents, *Green Chemistry*, **9**(9): 927–934, doi: 10.1039/B617536H.
11. Choi W., Choudhary N., Han G.H., Park J., Akinwande D., Hee-Lee Y. (2017), Recent development of two-dimensional transition metal dichalcogenides and their applications, *Materials Today*, **20**(3): 116–130, doi: 10.1016/j.mattod.2016.10.002.
12. Coleman J.N. *et al.* (2011), Two-dimensional nanosheets produced by liquid exfoliation of layered materials, *Science*, **331**(6017): 568–571, doi: 10.1126/science.1194975
13. Connors K.A., Wright J. (1989), Dependence of surface tension on composition of binary aqueous-organic solutions, *Analytical Chemistry*, **61**(3): 194–198, doi: 10.1021/ac00178a001.
14. Ebrahiminia A., Mokhtari-Dizaji M., Toliyat T. (2013), Correlation between iodide dosimetry and terephthalic acid dosimetry to evaluate the reactive radical production due to the acoustic cavitation activity, *Ultrasonics Sonochemistry*, **20**: 366–372, doi: 10.1016/j.ultsonch.2012.05.016.
15. Frisenda R. *et al.* (2016), Micro-reflectance and transmittance spectroscopy: A versatile and powerful tool to characterize 2D materials, *Journal of Physics D: Applied Physics*, **50**(7): 074002, doi: 10.1088/1361-6463/aa5256.
16. Ghasemi F., Mohajerzadeh S. (2016), Sequential solvent exchange method for controlled exfoliation of MoS_2 suitable for phototransistor fabrication, *ACS Applied Materials & Interfacesaces*, **8**(45): 31179–31191, doi: 10.1021/acsami.6b07211.
17. Hajnorouzi A., Afzalzadeh R., Ghanati F. (2014), Studies on the regularity of wave intensity in ultrasonic bath and spherical reactor, *Journal of Acoustical Engineering Society of Iran*, **2**(1): 32–39.
18. Han J.T. *et al.* (2014), Extremely efficient liquid exfoliation and dispersion of layered materials by unusual acoustic cavitation, *Scientific Reports*, **4**(1): 5133, doi: 10.1038/srep05133.
19. Han S.A., Bhatia R., Kim S-W. (2015), Synthesis, properties and potential applications of two-dimensional transition metal dichalcogenides, *Nano Convergence*, **2**(1): 17, doi: 10.1186/s40580-015-0048-4.
20. Huo C., Yan Z., Song X., Zeng H. (2015), 2D materials via liquid exfoliation: a review on fabrication and applications, *Science Bulletin*, **60**(23): 1994–2008, doi: 10.1007/s11434-015-0936-3.
21. Jawaid A. *et al.* (2016), Mechanism for liquid-phase exfoliation of MoS_2, *Chemistry of Materials*, **28**(1): 337–348, doi: 10.1021/acs.chemmater.5b04224.
22. Kajbafvala M., Farbod M. (2018), Effective size selection of MoS_2 nanosheets by a novel liquid cascade centrifugation: Influence of the flakes dimensions on electrochemical and photoelectrochemical applications, *Journal of Colloid and Interface Science*, **527**: 159–171, doi: 10.1016/j.jcis.2018.05.026.
23. Kiełczyński P., Ptasznik S., Szalewski M., Balcerzak A., Wieja K., Rostocki A.J. (2019), Application of ultrasonic methods for evaluation of high-pressure physicochemical parameters of liquids, *Archives of Acoustics*, **44**(2): 329–337, doi: 10.24425/aoa.2019.128496.
24. Kudryashova O.B., Vorozhtsov A., Danilov P. (2019), Deagglomeration and coagulation of particles in liquid metal under ultrasonic treatment, *Archives*

of Acoustics, **44**(3), 543–549, doi: 10.24425/aoa.2019.129269.

25. Liu Y.D. *et al.* (2013), Preparation, characterization and photoelectrochemical property of ultrathin MoS_2 nanosheets via hydrothermal intercalation and exfoliation route, *Journal of Alloys and Compounds*, **571**: 37–42, doi: 10.1016/j.jallcom.2013.03.031.
26. Mak K.F., Lee C., Hone J., Shan J., Heinz T.F. (2010), Atomically thin MoS_2: A new direct-gap semiconductor, *Physical Review Letters*, **105**(13): 136805, doi: 10.1103/physrevlett.105.136805
27. Marcus Y. (2018), Extraction by subcritical and supercritical water, methanol, ethanol and their mixtures, *Separations*, **5**(1): 4, doi: 10.3390/separations5010004.
28. Mas-Ballesté R., Gómez-Navarro C., Gómez-Herrero J., Zamora F. (2011), 2D materials: to graphene and beyond, *Nanoscale*, **3**(1): 20–30, doi: 10.1039/C0NR00323A.
29. Merouani S., Hamdaoui O., Rezgui Y., Guemini M. (2013), Effects of ultrasound frequency and acoustic amplitude on the size of sonochemically active bubbles – theoretical study, *Ultrasonics Sonochemistry*, **20**(3): 815–819, doi: 10.1016/j.ultsonch.2012.10.015.
30. Miró P., Audiffred M., Heine T. (2014), An atlas of two-dimensional materials, *Chemical Society Reviews*, **43**(18): 6537–6554, doi: 10.1039/C4CS00102H.
31. Nguyen E.P. *et al.* (2015), Investigation of two-solvent grinding-assisted liquid phase exfoliation of layered MoS_2, *Chemistry of Materials*, **27**(1): 53–59, doi: 10.1021/cm502915f.
32. Nguyen T.P., Sohn W., Oh J.H., Jang H.W., Kim S.Y. (2016), Size-dependent properties of two-dimensional MoS_2 and WS_2, *The Journal of Physical Chemistry C*, **120**(8): 10078–10085, doi: 10.1021/acs.jpcc.6b01838.
33. Nicolosi V., Chhowalla M., Kanatzidis M.G., Strano M.S., Coleman J.N. (2013), Liquid exfoliation of layered materials, *Science*, **340**(6139): 1226419-(1–18), doi: 10.1126/science.1226419.
34. Niu Y. *et al.* (2018), Thickness-dependent differential reflectance spectra of monolayer and few-layer MoS_2, $MoSe_2$, WS_2 and WSe_2, *Nanomaterials*, **8**(9): 725, doi: 10.3390/nano8090725.
35. Peng J., Weng J. (2015), One-pot solution-phase preparation of a MoS_2/graphene oxide hybrid, *Carbon*, **94**: 568–576. doi: 10.1016/j.carbon.2015.07.035.
36. Pokhrel N., Vabbina P.K., Pala N. (2016), Sonochemistry: Science and Engineering, *Ultrasonics Sonochemistry*, **29**: 104–128, doi: 10.1016/j.ultsonch.2015.07.023.
37. Qiao W. *et al.* (2014), Effects of ultrasonic cavitation intensity on the efficient liquid-exfoliation of MoS_2 nanosheets, *RSC Advances*, **4**(92): 50981–50987, doi: 10.1039/C4RA09001B.
38. Samadi M., Sarikhani N., Zirak M., Zhang H., Zhang H-L., Moshfegh A.Z. (2018), Group 6 transition metal dichalcogenide nanomaterials: synthesis, applications and future perspectives, *Nanoscale Horizons*, **3**(2): 90–204, doi: 10.1039/C7NH00137A.
39. Shen J. *et al.* (2015), Liquid phase exfoliation of two-dimensional materials by directly probing and matching surface tension components, *Nano Letters*, **15**(8): 5449–5454, doi: 10.1021/acs.nanolett.5b01842.
40. Song X., Hub J., Zeng H. (2013), Two-dimensional semiconductors: recent progress and future perspectives, *Journal of Materials Chemistry C*, **1**(17): 2952–2969, doi: 10.1039/C3TC00710C.
41. Tamura R., Miyata M. [Eds] (2015), *Advances in Organic Crystal Chemistry: Comprehensive Reviews*, Springer, doi: 10.1007/978-4-431-55555-1.
42. Tonndorf P. *et al.* (2013), Photoluminescence emission and Raman response of monolayer MoS_2, $MoSe_2$, and WSe_2, *Optics Express*, **21**(4): 4908–4916, doi: 10.1364/OE.21.004908.
43. Vella D. *et al.* (2016), Femtosecond spectroscopy on MoS_2 flakes from liquid exfoliation: surfactant independent exciton dynamics, *Journal of Nanophotonics*, **10**(1): 012508-1–012508-8. doi: 10.1117/1.JNP.10.012508.
44. Voshell A., Terrones M., Rana M. (2018), Review of optical properties of two-dimensional transition metal dichalcogenides, *Proceedings of SPIE 10754, Wide Band gap Power and Energy Devices and Applications III*, 107540L, doi: 10.1117/12.2323132
45. Wang F. *et al.* (2015), Synthesis, properties and applications of 2D non-graphene materials, *Nanotechnology*, **26**(29): 292001, doi: 10.1088/0957-4484/26/29/292001.
46. Wang Q.H., Kalantar-Zadeh K., Kis A., Coleman J.N., Strano M.S. (2012), Electronics and optoelectronics of two-dimensional transition metal dichalcogenides, *Nature Nanotechnology*, **7**(11): 699–712, doi: 10.1038/nnano.2012.193.
47. Wang Z.M. (2014), *MoS_2-Materials, Physics, and Devices. Lecture Notes in Nanoscale Science and Technology*, Vol. 21, Springer International Publishing, Switzerland, doi: 10.1007/978-3-319-02850-7.
48. Xu H., Zeiger B.W., Suslick K.S. (2013), Sonochemical synthesis of nanomaterials, *Chemical Society Reviews*, **42**(7): 2555–2567, doi: 10.1039/C2CS35282F.
49. Yang L. *et al.* (2018), Properties, preparation and applications of low dimensional transition metal dichalcogenides, *Nanomaterials*, **8**(7): 463, doi: 10.3390/nano8070463.
50. Zhang G., Liu H., Qu J., Li J. (2016), Two-dimensional layered MoS_2: rational design, properties and electrochemical applications, *Energy & Environmental Science*, **9**: 1190–1209, doi: 10.1039/C5EE03761A.
51. Zhu J. *et al.* (2016), Thickness-dependent bandgap tunable molybdenum disulfide films for optoelectronics, *RSC Advances*, **6**: 110604–110609, doi: 10.1039/C6RA22496B.